High-Fidelity Numerical Simulations of Range-Resolved, Time-Varying Radar Backscatter from a Sea Surface with Floating Targets

Jakov V. Toporkov and Mark A. Sletten
Remote Sensing Division, Code 7264, US Naval Research Laboratory
4555 Overlook Ave, SW, Washington, DC, 20375, USA

jakov.toporkov@nrl.navy.mil mark.sletten@nrl.navy.mil

ABSTRACT

Time-dependent properties of coherent range-resolved backscatter from a sea surface with simple floating targets are studied using two-dimensional (2-D) direct numerical simulations based on a first-principles boundary integral equation technique. The deterministic sea surface is generated according to a wind-driven wave spectrum. Target motion is modeled in a simplified way as that of a massless object heaved by orbital currents. Calculations can be performed at a broad range of grazing angles, and at both HH and VV polarizations. The paper gives examples of range-time records of the X-band backscatter and then focuses on the Doppler characteristics of the simulated received signals. Differences between the responses of floating targets and the sea surface are rather conspicuous and appear to be caused primarily by dissimilarities in cross-section modulation behavior. These distinctions in Doppler signatures can form the basis for target detection against the clutter, and the "numerical experiment" has the advantage of providing benchmark data sets collected under highly controlled conditions. The studies can be further refined by considering more sophisticated target motion models, as well as accounting for the disturbance of ambient water waves by the floating object.

1.0 INTRODUCTION

The ship-board or airborne detection of low-observable targets on the sea surface is an important problem for the Navy. Radar echoes from such objects are often buried in the ambient sea clutter, with the latter tending to have a spiky nature, especially towards low grazing-angles [1]. Hence, the traditional magnitude threshold detection approach can be problematic. Yet, in all likelihood, target echoes have spatial, temporal, and polarimetric correlation properties that differ from those of the sea clutter, and these differences could be exploited in advanced detection algorithms. Knowledge and understanding of such detailed, comprehensive characteristics of radar backscatter coming from sea surface and from various classes of targets is a key to success.

Direct numerical simulations have proven to be a useful tool to investigate sea surface backscatter [2]-[6]. The approach is based on solving the first-principles boundary integral equation for the induced electric current on a given deterministic surface profile. It inherently accounts for multiple scattering and shadowing effects and yields an exact answer for the scattered field for any grazing angle. The boundary profile (sea surface that may include targets) itself is generated and evolved according to a suitable physical model. The technique is limited to the 2-D space, but is relevant in rather commonly occurring three-dimensional geometries, such as a radar observing approaching long-crested waves. The numerical experiment, with its ability to produce noise-free, calibrated datasets of complex sea backscatter under well-controlled conditions, offers rather unique opportunities for comprehensive high-fidelity analysis.

In this paper we consider X-band short-pulse backscatter from an evolving sea-like surface with floating semi-submerged spherical objects. Examples of the simulated time-range records of radar echoes at various grazing angles are shown. We then focus on the Doppler analysis of the complex received signals in a single range bin corresponding to the target location. The numerical simulations allow generating and comparing the data

corresponding to the same evolving sea surface profile with or without the target. This provides insights into the similarities and distinctions of the "target+clutter" and "clutter" Doppler signatures. Generally, it is observed that the average Doppler centroids at the target locations are noticeably different from those coming from other, "surface only" range bins. This is true for a variety of grazing angles and near-surface wind speeds (sea states). Such a distinction can be exploited for detection of this class of round floating targets.

2.0 SIMULATION DETAILS

Numerical simulations of ocean scattering include two distinct components. The ability to evaluate the electromagnetic field scattered by a surface with any given profile (with or without embedded target) is one crucial element. In addition, the surface profiles should emulate the ocean roughness (generally, inherently random) as it develops through wave-wind and wave-wave interactions. The level of surface detail is dictated by the radar wavelength. If floating targets are considered, their motion should also be realistically modeled. Fig. 1-1 illustrates the setup geometry, and the simulations components are discussed below.

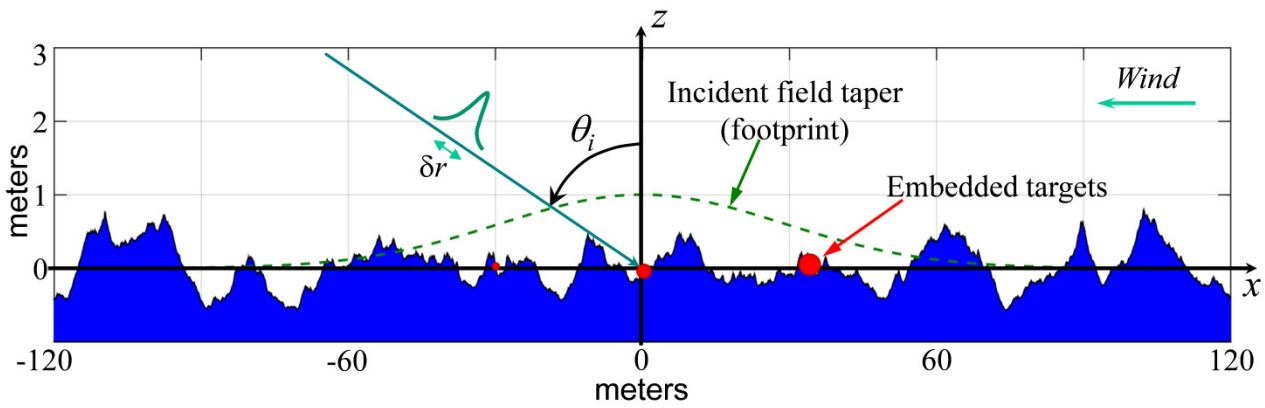

Figure 1-1: Problem setup.

2.1 Modelling Sea Surface and Floating Objects

As in a number of previous studies, e.g. [2]-[6], generation of a deterministic sea surface starts with a realization of a stationary Gaussian random process. The power spectral density of the latter is modelled here after the fully developed Elfouhaily wave spectrum [7] that has the wind speed at 10 m above the surface as the governing parameter. Specifically, the prototype surface at a start time is a linear superposition of harmonics whose amplitudes are independent Gaussian-distributed complex random numbers with variances defined by the surface spectrum. For temporal evolution, each harmonic in the realization is propagated independently of all others according to water-wave dispersion relation [2]. To account for hydrodynamic interactions between long and short waves, the prototype linear surface profile at every time step undergoes a transformation due to Creamer [8]. While the method leaves out any wave breaking, the notable effects include sharper wave crests/shallower troughs (which is a manifestation of more realistic non-Gaussian surface statistics) and a modified dispersion relation. In this report we will mainly consider 7-m/s surfaces, but the simulations have been conducted at other wind speeds (5 m/s and 10 m/s). The time step between the "frozen" profiles that represent the surface evolution is 2×10^{-3} s.

The targets to be embedded have a simple round shape and are presumed to be mostly submerged. The dynamics of their floating motions and the interactions with the ambient surface (e.g. generating splash) could be important for radar signature. These aspects can be refined using motion and hydrodynamic models of

varying degree of complexity. Here we consider a rather simple case: a floating object behaves as a massless body heaved by the waves' orbital currents, and except for eliminating the surface roughness where broached, the target does not affect or modify the surrounding surface. The latter means that there is no wave diffraction on the target and no secondary wave creation by the target.

Under these assumptions generation of surface profiles with the embedded targets proceeds as follows. First, one produces a sequence representing temporal evolution of a given surface realization in the absence of any targets. In terms of continuous variables the time-evolving surface height can be expressed as

$$\zeta(x,t) = \mathrm{Re}\left\{\frac{1}{2\pi}\int_{-\infty}^{\infty}\hat{\zeta}(K,t)e^{jKx}dK\right\} \tag{1}$$

with $\hat{\zeta}(K,t)$ representing the directional Fourier spectrum of the surface at time t (i.e. its values for $K>0$ describe the waves travelling in the positive-x direction and vice versa). The translational motion of the round object is specified entirely by the displacement of its center, which we assume to be moving with the orbital current. From the *linear* wave theory, the horizontal and vertical components of the orbital current at the depth $z<0$ are given by

$$v_x(x,z,t) = \mathrm{Re}\left\{\frac{1}{2\pi}\int_{-\infty}^{\infty}\mathrm{sign}(K)\Omega(K)e^{|K|z}\hat{\zeta}(K,t)e^{jKx}dK\right\} \tag{2a}$$

and

$$v_z(x,z,t) = \mathrm{Im}\left\{\frac{1}{2\pi}\int_{-\infty}^{\infty}\Omega(K)e^{|K|z}\hat{\zeta}(K,t)e^{jKx}dK\right\} \tag{2b}$$

Above,

$$\Omega(K) = \sqrt{g|K|} \tag{3}$$

is the gravity-wave dispersion relation (g is the gravity acceleration). In principle, one can include the capillary part as well (cf. [2]), but those short waves generally won't play any appreciable role. Although strictly speaking, (2) is based on the linear wave theory, we use the Creamer-modified non-linear surface spectrum $\hat{\zeta}(K,t)$. The nominal placement of the target, assuming the non-disturbed flat surface, is (x_0,z_0). The spatial evolution of its center in the presence of the surface is evaluated by numerically integrating the velocities in (2); the depth on the right-hand side is kept at $z=z_0$. The reasonable initial position of the target center at $t=0$, when the surface is rough, can be determined by analytically integrating (2) in time (starting from $t=-\infty$ when the surface is presumed undisturbed) assuming the linear wave theory [9]. Knowing the location of the center and the target radius, a simple code can evaluate the broached region and form the synthetic "target+surface" profile, shown in Fig. 1-2. Table 1-1 summarizes the parameters of the embedded targets (the horizontal location x_0 and the center depth z_0 are specified assuming flat unperturbed surface).

2.2 Electromagnetic Calculations

Scattered electromagnetic field from each surface profile is calculated exactly, using a frequency-domain boundary integral equation formulation for the induced surface current. The equation is solved iteratively using the Method of Ordered Multiple Interactions (MOMI), also known as Forward-Backward (FB) technique; further computational acceleration can be achieved by applying spectral expansions to the kernels (propagators) [10].With an embedded object, one may need to employ the Generalized FB method [11] that allows for an

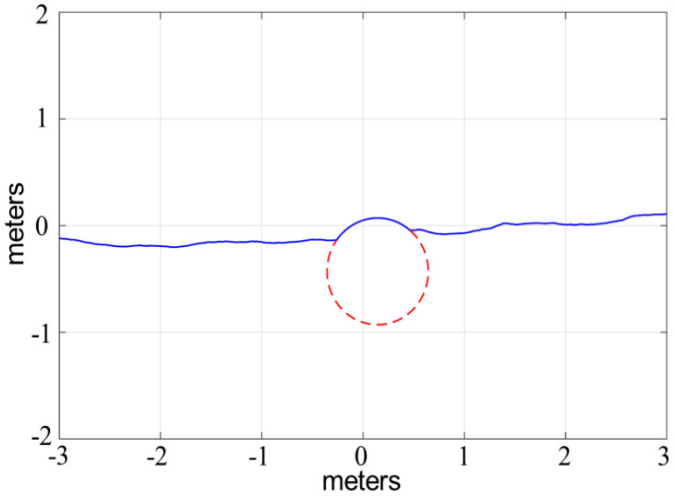

Figure 1-2: Close-up view of a surface profile with a semi-submerged floating target.

Table 1-1: Parameters of the embedded targets.

#	Diameter d, m	Location x, m	Center depth
1	1.0	0	$d/3$
2	1.5	35	$d/3$
3	0.5	-30	$d/3$

arbitrary target shape. However, for the simple low-profile bodies that we consider, no such modification to the solution scheme is necessary and the regular FB method still works well. The incident field at the surface acts as a forcing term in the integral equation and is assumed to be a tapered plane wave, with the angle of incidence (or grazing) being a principal characteristic, cf. Fig.1-1. Once the total induced current on the surface is found, the scattered field anywhere in the upper half-space can be calculated as its radiation effect by applying the appropriate propagator. We will focus on backscattering in the far-field region.

The frequency-domain formulation assumes that all fields and currents are time-harmonic. To achieve range resolution, the simulations are performed for a number of frequencies (2048 in all) covering the band of 1.25 GHz around f_0=10 GHz (λ_0=3 cm). Application of a spectral window combined with the inverse Fourier transform results in the synthesized surface response to a short pulse with the corresponding envelope. In particular, the choice of the Harris-Nutall spectral weighing [3] yields the pulse with very low sidelobes and the effective duration (measured by signal magnitude) as short as 2.25 ns. This corresponds to the range resolution of 0.34 m. Both VV and HH-polarized returns can be produced for the same scattering profile.

The steps described above are repeated for each surface or surface+targets profile in the sequence representing the temporal evolution [2], [4]. The outcome is a record of the range-resolved coherent radar returns from the simulated evolving sea-like surface with floating objects. Note that unlike the real-world measurements the results of the numerical experiment are free from thermal noise, although the latter may be subsequently generated and added to the data. Finally, it should be kept in mind that we are dealing with the 2-D configuration, so in terms of the 3-D space the targets represent infinitely long cylinders, while the antenna pattern in the azimuth (y) direction is very narrow.

3.0 RESULTS AND DISCUSSION

3.1 Example of Simulated Backscatter

Fig. 1-3 shows time-range intensity plots of the HH-polarized radar backscatter from the same evolving 7-m/s surface with the targets (cf. Table 1-1) when observed from various grazing angles. (The grazing angle θ_{gr} is complementary to the incidence angle θ_I shown in Fig. 1-1). The vertical axis is converted to the ground range that corresponds to the x-coordinate in Fig. 1-1. The data are synthesized with the finest range

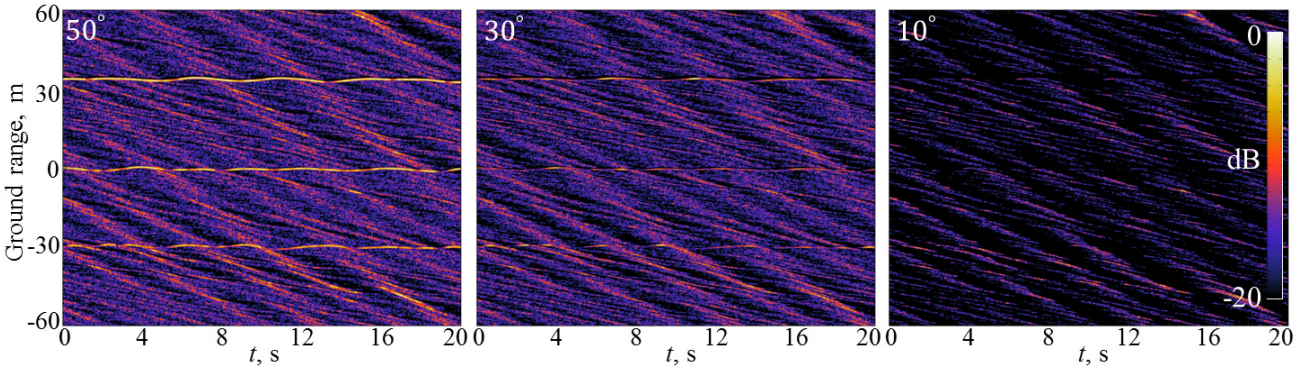

Figure 1-3. Backscatter magnitude from a 7-m/s surface with targets (dB scale, each plot normalized to its own maximum) for three values of grazing angle. HH polarization, range resolution is 0.34 m.

resolution of 0.34 m, and the modulation associated with the incident field taper ("antenna pattern") has been removed. At high grazing angle (50°) all three targets are very well visible through the entire 20-s record duration. Their backscatter appears to have a specular-reflection nature that dominates the resonance (tilted Bragg) mechanisms that are at play in scattering by the surrounding sea surface. At this grazing angle, it appears, the exposed (broached) part of the round body almost all the time contains a point that satisfies the specular backreflection condition. This is no longer the case for the 30° grazing angle, as the target echoes become more intermittent in time. Interestingly, for a larger target (around the ground range mark of 35 m) one can notice a dark band on the farther side, as the area facing away from the radar and not producing any backreflection now gets resolved. Finally, at low grazing angles (10°) the targets do not seem to yield any noticeable backscatter. It should be noted that the time dimension (and the length of time record) plays an important role in the target signatures in the Figure being obvious to the naked eye. If the observer were presented with only, say, the first second of the 30°-grazing data record in Fig.1-3, the existence of backscatter anomalies (indicative of targets) would not be as apparent, at least for the smaller objects 1 and 3.

3.2 Doppler Spectrograms from a Single Range Bin

As the simulations produce coherent complex backscatter (containing both magnitude and phase), one can investigate the Doppler properties of the received echoes. Fig. 1-4a shows the behavior of the Doppler spectrum evaluated for the complex data transect corresponding to the ground range of 34.5 m, where the larger target 2 is located. To reduce the effects of the target moving in and out of the range bin (as is apparent in Fig. 1-3), the simulated radar responses were synthesized with a coarser resolution of 1 m. The grazing angle in this case is 20°. The spectrum was evaluated using a sliding window w :

$$D(f_d, t, x_g) = \left| \int_{-\infty}^{\infty} w(t'-t)s(t', x_g)e^{-j2\pi f_d t'} dt' \right|, \quad (4)$$

with $s(t, x_g)$ being the complex signal at the range bin (labelled by the ground range x_g) of interest. The function w was chosen to be a 256-point Hann window; with the "slow time" step between the simulated returns of 2×10^{-3} s (corresponding to the "pulse repetition frequency" of 500 Hz) this amounts to the total window width of 0.512 s. Practical implementation of (4) leading to the plots in Fig. 1-4 accounted for the fact that the signal s was available only for the duration of 20 s, and the values of D were retained only for times t where the sliding window in the integrand fully overlapped with the signal. The observed excursions of the instantaneous Doppler spectrum must be indicative of the undulating motion that the floating body is

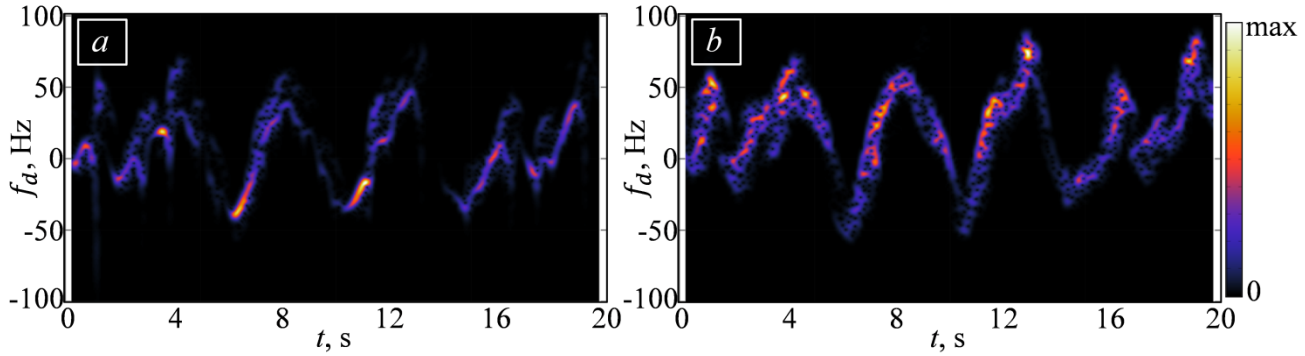

Figure 1-4. Magnitudes of the HH-pol Doppler spectra evaluated along the ground range cut $x_g = 34.5$ m with a sliding time window. a) Target present; b) target absent (sea surface only). Linear scale, with each plot normalized to its own maximum. Wind speed is 7 m/s, grazing angle equals 20°. resolution is 1.0 m.

experiencing as it is heaved by the passing waves.

The numerical experiment offers a unique and precise comparison of this target signature with that from the sea surface. As described earlier, the scattering simulations can be repeated with the same set of surface profiles with no targets embedded. The spectrum evaluated for such a case at exactly the same ground range is shown in Fig. 1-4b. Given the present method of the floating object implanting, here we largely observe the response from the surface roughness that was eliminated by the broached part of the target in the previous example. Looking at both panels in Fig. 1-4, one notices similarities in the trajectories traced by the spectra. This is not entirely surprising, as both the target and the surface ripples that it replaced are similarly hauled by the orbital currents from long waves. The surface-only spectrogram seems to have larger width along the frequency axis, although the difference is not particularly dramatic. However, there is yet another distinction. One can notice that in the "surface only" case the large spectral values tend to occur towards large positive frequencies (characteristic of motion towards the radar), while in the presence of a target this is not the case and the spectrogram tends to peak towards negative frequencies. This is indicative of the differences in cross section modulation between the round body and a rough surface patch both riding the same long waves. For the ocean surface, the concept of the "modulation transfer function" (MTF) has been studied extensively [12]; the main mechanism behind the normalized cross section variation would be changing slope (tilt) of a Bragg-scattering facet, with larger local incidence angle usually leading to weaker backscatter. As mentioned, for a round object the main scattering mechanism would involve a specular-point backreflection, and the strength of this reflection should be rather constant as long as there is a specular point. The reason the spectrogram in Fig. 1-4a still has spotty maxima must be due to the target (or rather, the specular point on the target) moving in and out of the chosen range bin. This scattering peculiarity, along with the inherent frequency shift due to propagating Bragg ripples in the "surface only" case, have even more obvious impact when one considers averaged Doppler spectrum.

3.3 Average Doppler Spectra vs. Range

Let us form the average Doppler spectrum for each range bin by summing up in time (in the root mean square sense) all the instantaneous spectra:

$$D_a(f_d, x_g) = \left[\frac{1}{T_D}\int_{-\infty}^{\infty} D^2(f_d, t, x_g)dt\right]^{\frac{1}{2}}. \quad (5)$$

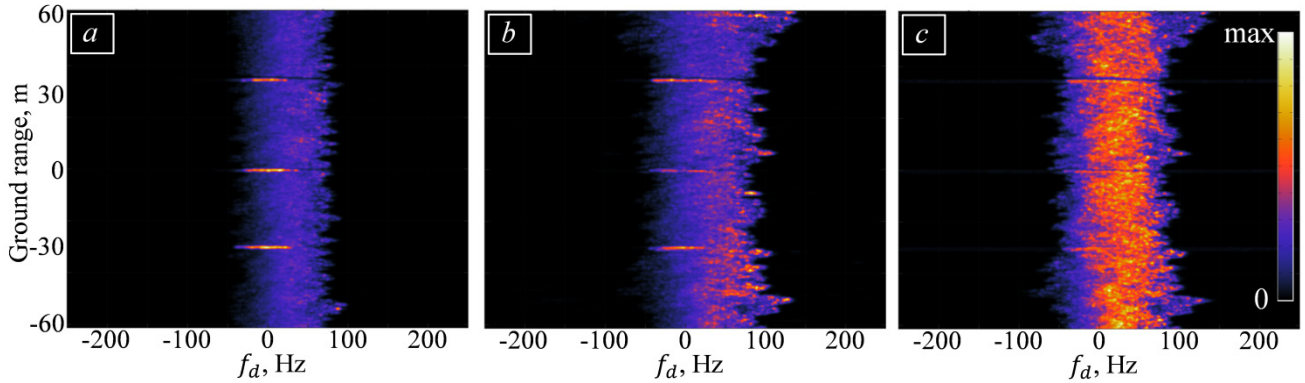

Figure 1-5. Averaged Doppler spectra vs. range for the backscatter from sea surface with targets: a) wind speed 5 m/s, HH-pol; b) wind speed 7 m/s, HH-pol; c) wind speed 7 m/s, VV-pol. Linear scale, with each plot normalized to its own maximum. Grazing angle equals 20°. resolution is 1.0 m.

In the formula above, T_D is the available duration of the spectrogram D; it equals the length of the original data record (20 s) reduced by the size of the applied sliding window (0.512 s). The plots corresponding to various surface and radar parameters are shown in Fig 1-5. As in Fig. 1-3, the vertical axis refers to the ground range, while the horizontal axis is now tracking the Doppler frequency. For the HH polarization (Figs. 1-5a,b), the average spectra in the range bins around target placements clearly stand out from the rest – both in terms of the amplitude and the center frequency. This is true for a variety of wind speeds (with Fig. 1-5b corresponding to the 7-m/s example considered in the previous section). At VV polarization (Fig. 1-5c) the Doppler spectrum for the ambient surface appears to be both stronger and centered closer to the frequency origin, thus the contrast with the target-containing range bins lessens. At higher grazing angles (moving closer to nadir) the qualitative picture for the average HH Doppler spectra persists. At the same time the VV-polarized plots become more resembling of their HH counterparts, with the spectra in the target-containing range bins increasingly standing apart from the rest that contain sea backscatter only. The particular choice of an averaging procedure (e.g. the type and size of the sliding window w) described in this study is not critical; in fact, similar conclusions would be reached if one considered a periodogram evaluated over the entire 20-s interval.

It is somewhat remarkable that these differences in the average Doppler spectra are observed even though the simple model of a floating body used here almost assures the similarity between its motion and that of the corresponding rough surface patch that the broached part replaces. These Doppler distinctions can certainly be exploited in detection of such floating round targets against the background surface. The qualitative discussion in the previous section suggests that at medium and high grazing angles the MTF approach [12] can be applied if further theoretical analysis is necessary. It is also worth reiterating that having and using a long backscatter record (spanning several dominant wave periods) is important. Otherwise the average spectra such as those shown in Fig. 1-5 would have significant centroid fluctuations with range and it would be hard to tell the difference between the target-containing bins from the "ambient surface only" ones.

4.0 CONCLUSION

Direct numerical simulations provide a capable and precise tool for investigating and understanding various aspects of radar backscatter in sea environment. Previous studies demonstrated the utility of numerical experiment for analyzing various statistical and temporal properties of sea backscatter and establishing dependencies of those characteristics on environmental and radar parameters. This study focuses on the Doppler properties of range-resolved backscatter from a see surface that contains semi-submerged floating

round targets. The task poses a new problem of adequately modelling the motion of a body as it responds to the incoming waves, and, in principle, accounting for the object's impact on the ambient wave field. At this point, a simple model was used assuming that the submerged center of the body follows the orbital currents associated with the water waves. This obviously disregards any inertia and should approximate the behavior of a light target in a viscous fluid. Any possible wave diffraction or wave generation by the target at this stage are also ignored, with the broached part of the body simply replacing the corresponding patch of the surface roughness in the model. Even in this basic case the simulations predict that away from the low grazing regime the targets will be visible to a radar, with their Doppler signature being quite different from that of the sea surface itself. This dissimilarity can be utilized to facilitate detection of such objects. The future work would involve development and incorporation of more sophisticated models for target floating motion and the associated perturbations of the surrounding sea surface. The latter aspect can be useful in investigating possible visibility of these smooth round targets at low grazing angles. Data sets generated by the numerical simulations can also serve as benchmark test inputs to evaluate and improve existing or prospective detection algorithms.

5.0 ACKNOWLEDGMENT

This work was supported by the US Naval Research Laboratory under the 6.2 Base Research Program (Work Unit 72-6891). It was also supported in part by a grant of computer time from the DoD High Performance Computing Modernization Program at the DoD Supercomputing Resource Centers at the US Air Force Research Laboratory, the US Army Research Laboratory and the US Army Engineering Research and Development Center, and at the Maui High Performance Computing Center.

[1] K. D. Ward, R. J. A. Tough, and S. Watts, *Sea Clutter: Scattering, the K distribution and Radar Performance*, London: The Institution of Engineering and Technology, 2006.

[2] J. V. Toporkov and G. S. Brown, "Numerical simulations of scattering from time varying, randomly rough surfaces," *IEEE Trans. Geosci. Remote Sensing*, vol. 38, pp. 1616-1625, 2000.

[3] J. V. Toporkov and M. A. Sletten, "Statistical properties of low-grazing range-resolved sea surface backscatter generated through two-dimensional direct numerical simulations," *IEEE Trans. Geosci. Remote Sensing*, vol.45, pp. 1181-1197, 2007.

[4] J. V. Toporkov and M. A. Sletten, "Numerical simulations and analysis of wide-band range-resolved HF backscatter from evolving ocean-like surfaces," *IEEE Trans. Geosci. Remote Sensing*, vol.50, pp. 2986-3003, 2012.

[5] J. V. Toporkov and M. A. Sletten, "Joint magnitude and phase properties of numerically simulated high-resolution VV- and HH-polarized X-band sea backscatter over wide range of incidence angles," *Proc. IEEE International Geoscience and Remote Sensing Symposium*, Quebec, CANADA, pp. 5025-5028, July 2014.

[6] J. T. Johnson, R. T, Burkholder, J. V. Toporkov, D. R. Lyzenga, and W. J. Plant, "A numerical study of the retrieval of sea surface height profiles from low grazing angle radar data," *IEEE Trans. Geosci. Remote Sensing*, vol.47, pp. 1641-1650, June 2009.

[7] T. Elfouhaily, B. Chapron, K. Katsaros, and D. Vandemark, "A unified directional spectrum for long and

short wind-driven waves," *J. Geophys. Res.*, vol. 102, no. C7, pp. 15781–15796, 1997.

[8] D. B. Creamer, F. Henyey, R. Schult, and J. Wright, "Improved linear representation of ocean surface waves," *J. Fluid Mech.*, **205**, pp. 135-161, 1989.

[9] J. J Stoker, *Water Waves,* New York: Interscience Publishers, pp. 45-47, 1957.

[10] H.-T. Chou and J. T. Johnson, "Formulation of Forward–Backward method using novel spectral acceleration for the modeling of scattering from impedance rough surfaces," *IEEE Trans. Geosci. Remote Sens*., vol. 38, pp. 605–607, 2000.

[11] M. R. Pino, L. Landesa, J. L. Rodriguez, F. Obelleiro, and R. J. Burkholder, "The generalized Forward-Backward method for analyzing the scattering from targets on ocean-like rough surfaces," *IEEE Trans. Antennas Propagat.,* vol. 47, pp. 961-969, 1999.

[12] R. Romeiser and D.R. Thompson, "Numerical study on the along-track interferometric radar imaging mechanism of oceanic surface current," *IEEE Trans. Geosci. Remote Sensing*, vol. 38, pp. 446-458, 2000.